AIAA 2003-0653

Wind Tunnel Database Development using Modern Experiment Design and Multivariate Orthogonal Functions

Eugene A. Morelli
NASA Langley Research Center
Hampton, VA

Richard DeLoach
NASA Langley Research Center
Hampton, VA

41st AIAA Aerospace Sciences Meeting and Exhibit
January 6-9, 2003 / Reno, NV

WIND TUNNEL DATABASE DEVELOPMENT USING MODERN EXPERIMENT DESIGN AND MULTIVARIATE ORTHOGONAL FUNCTIONS

Eugene A. Morelli* and Richard DeLoach†

NASA Langley Research Center
Hampton, Virginia USA 23681 – 2199

Abstract

A wind tunnel experiment for characterizing the aerodynamic and propulsion forces and moments acting on a research model airplane is described. The model airplane, called the Free-flying Airplane for Sub-scale Experimental Research (FASER), is a modified off-the-shelf radio-controlled model airplane, with 7 ft wingspan, a tractor propeller driven by an electric motor, and aerobatic capability. FASER was tested in the NASA Langley 12-foot Low-Speed Wind Tunnel, using a combination of traditional sweeps and modern experiment design. Power level was included as an independent variable in the wind tunnel test, to allow characterization of power effects on aerodynamic forces and moments. A modeling technique that employs multivariate orthogonal functions was used to develop accurate analytic models for the aerodynamic and propulsion force and moment coefficient dependencies from the wind tunnel data. Efficient methods for generating orthogonal modeling functions, expanding the orthogonal modeling functions in terms of ordinary polynomial functions, and analytical orthogonal blocking were developed and discussed. The resulting models comprise a set of smooth, differentiable functions for the non-dimensional aerodynamic force and moment coefficients in terms of ordinary polynomials in the independent variables, suitable for nonlinear aircraft simulation.

Nomenclature

$\boldsymbol{a}$	parameter vector
C_L, C_D, C_Y	lift, drag, and side force coefficients
C_l	rolling moment coefficient
C_m	pitching moment coefficient
C_n	yawing moment coefficient
$\boldsymbol{Cov}$	covariance matrix
J	cost function
MDOE	Modern Design Of Experiments
n	number of model terms
N	total number of data points
OFAT	One Factor At a Time
PSE	predicted squared error
pwr	power level, percent
$\boldsymbol{p}$	modeling function vector
T	thrust force, lbf
$\boldsymbol{x}$	independent variable vector
$\boldsymbol{y}$	measured output vector
α	angle of attack, deg
β	sideslip angle, deg
δ_a	aileron deflection, deg
δ_e	elevator deflection, deg
δ_f	flap deflection, deg
δ_r	rudder deflection, deg
σ^2	variance
$\boldsymbol{\xi}$	ordinary polynomial function vector

superscripts

T	transpose
$\hat{}$	estimate
-1	matrix inverse
$\tilde{}$	normalized

* Research Engineer, Senior Member AIAA

† Senior Research Scientist

subscripts

max	maximum
min	minimum
o	nominal

Introduction

Modern aeronautical research involves expanded flight envelopes, as a result of the desire for improved fighter maneuverability for tactical advantages, and the desire to improve flight safety. The expanded flight envelopes involve nonlinear aerodynamics which must be modeled accurately.

Since nonlinear aerodynamics are much more complex than linear aerodynamics, more sophisticated experimentation is required to accurately characterize the functional dependencies. Nonlinear aerodynamics violate linear modeling assumptions such as superposition, quasi-steady flow, and no interdependence of the effects of states and controls. In addition, aircraft designs have evolved with increasing numbers of control effectors. Traditional wind tunnel testing methods would set each control effector to different fixed levels while sweeping through angle of attack and sideslip angle, for example. With such an approach, the number of data points required increases exponentially with the number of control effectors, if information on control surface interaction effects is desired. These considerations highlight the need to develop more efficient wind tunnel testing and modeling techniques to accurately characterize nonlinear aerodynamics, with possible interaction effects among a large number of independent variables.

At NASA Langley, the Free-flying Airplane for Sub-scale Experimental Research (FASER) is being developed to study problems such as that described above. FASER is a modified off-the-shelf radio control model called the Ultra-Stick, manufactured by Hangar 9, Ltd., see Figure 1. FASER has a conventional high-wing and tail configuration with 7 ft wingspan, a foldable tractor propeller driven by an electric motor, and aerobatic capability.

The purpose of FASER is to provide an inexpensive aircraft for developing and demonstrating advanced experiment design, data analysis and modeling techniques, and control law design methods. As long as the goal is technology demonstration or basic research, a sub-scale model that is not dynamically scaled for a specific full-scale aircraft is a completely acceptable test vehicle for these purposes.

FASER was designed so that the flight vehicle could be installed in the wind tunnel, see Figure 1. This avoids any Reynolds number or scaling effects, and ensures that there are no physical differences between the wind tunnel model and the flight vehicle.

In contrast, full scale flight tests and drop model tests are expensive and are sometimes separated by months (and even years) for a particular research activity. The number of these tests is always tightly constrained by budget. There is also a substantial difference in the cost of overhead if the aircraft is to be kept in flyable condition. Since FASER is inexpensive and unmanned, risks can be taken in research and development that could never be tolerated in a piloted flight test or even in a drop model test. Advances in instrumentation now make it possible to instrument a sub-scale model aircraft with research-quality, miniaturized flight test instrumentation at a reasonable cost.

This paper describes the experiment design, data analysis, and mathematical modeling involved in developing a wind tunnel database for the FASER aircraft. Accuracy of this database is critical for the development of a high-fidelity nonlinear simulation to be used for control law design, flight envelope expansion, flight experiment design, and pilot training. A preliminary version of the nonlinear simulation for FASER has already been developed, using U.S. Air Force DATCOM to generate an aerodynamic model, with experimentally-determined values for the mass and inertia characteristics of FASER[1]. The work described in this paper will upgrade the aerodynamic model with analytic models derived from wind tunnel data, add an engine thrust model, and include propulsion effects on the aerodynamics. Since FASER was intended to be a research vehicle from the outset, the approach used for the experiment design and data analysis for the wind tunnel testing was not traditional. This paper explains how the wind tunnel testing was done, and examines the results. The paper also describes a method for generating orthogonal modeling functions based on the independent variable data, along subsequent expansion of the orthogonal modeling functions in terms of ordinary multivariate polynomials. This method is slightly different from that described in Refs. [2] and [3], and represents an evolutionary improvement of the technique. In Ref. [2], the concept of response surface modeling using multivariate orthogonal functions was successfully applied to inference subspaces for limited ranges of

angle of attack and Mach number with fixed sideslip angle and control surface deflections. This paper extends the multivariate orthogonal function modeling concept to identify aerodynamic models for a large flight envelope, with more independent variables.

Experiment Design

For this wind tunnel test, the fundamental objective was to find a mathematical description for the dependence of non-dimensional aerodynamic force and moment coefficients on independent variables that are varied during the experiment. Each mathematical description or model can be thought of geometrically as a hyper-surface, also called a response surface. Critical issues for successfully identifying an adequate response surface model from experimental data include the experiment design (or, how the independent variable values are set when measuring the output responses), noise level on the measured outputs, identification of a mathematical model structure that can capture the functional dependence of the output variables on the independent variables, accurate estimates of unknown parameters in the identified model structure, and the ability of the identified model to predict outputs for data that was not used to identify the response surface model.

The experiment design used for FASER wind tunnel testing was a hybrid design broken down into a series of procedures. The procedures are listed in Table 1. Randomization[4-6] was used throughout the testing, to separate independent variable effects from time-dependent systematic errors.

The first procedure consisted of randomized engine power sweeps with the wind tunnel air off, to determine the static thrust from the electric motor and the propeller. All of these runs were made with the model at zero angle of attack and zero sideslip angle, so that the thrust measurement was obtained from the longitudinal force measured by the balance mounted in the model. Figure 2 shows the static thrust plotted as a function of pulses per second from a Hall effect transducer on the electric motor, which is proportional to the propeller RPM. The model shown in Figure 2 is the result of a simple least squares fit of thrust to pulse count, using a quadratic model structure. This model structure was identified automatically from the data, using the orthogonal function modeling technique described later.

In the second and third procedures, the approach was to use One Factor At a Time (OFAT) sweeps, wherein one independent variable is changed with all others held constant, to characterize the general topology of the response surfaces for the non-dimensional coefficients, get an idea of the response levels, collect basic static stability and trim information, and define the boundaries of the independent variable subspaces to be used for further experimentation. OFAT sweeps were used because the data acquisition system in the NASA Langley 12-foot Low-Speed Wind Tunnel is set up to collect OFAT data in an automated fashion, making the sweeps very efficient in terms of collecting data points in minimum time. However, the initial OFAT sweeps are really only intended for qualitative use, namely to define the boundaries for subspaces that will be the focus of detailed experimentation and modeling in procedure four. One advantage of operating in this manner is that any issues related to instrumentation, data collection, or experimental procedures can be worked out during the OFAT sweeps without impact on the experiment, because the data from the OFAT sweeps is being used for qualitative purposes only. This approach also provides a good rough overview of the landscape that characterizes the dependence of force and moment coefficients on the independent variables.

The independent variables for the FASER wind tunnel test were angle of attack α, sideslip angle β, power level *pwr*, elevator deflection δ_e, aileron deflection δ_a, rudder deflection δ_r, and flap deflection δ_f. The response variables were non-dimensional aerodynamic coefficients for lift, drag, and side forces $(C_L, C_D, \text{and } C_Y)$, and rolling, pitching, and yawing moments $(C_l, C_m, \text{and } C_n)$. Each data point produced measured values for all independent and response variables.

The experiment was designed assuming any of the independent variables could influence any of the response variables. It was assumed (as an initial guess only) that the dependencies could be modeled accurately with polynomial terms in the independent variables of order 3 or less within each independent variable subspace. In addition, it was assumed that longitudinal controls (δ_e, δ_f, and *pwr*) do not interact with lateral/directional controls (δ_a and δ_r). In practical terms, this meant that longitudinal and lateral/directional controls were not varied simultaneously to allow their mutual interaction effects to be quantified. As a result, the subspaces were called "longitudinal" if the longitudinal controls were moved, and "lateral/directional" if the lateral/directional controls were moved.

Based on experience with similar airplanes, it was known that the dependence of non-dimensional aerodynamic force and moment coefficients on control surface deflections could be modeled with low order polynomials for the entire range of control surface deflections. With that assumption, it was not necessary to vary the control surface deflections to search for inference subspace boundaries along the dimensions of the independent variable space corresponding to control surface deflections. Inference subspace boundaries were therefore sought only for α, β, and *pwr*. These independent variables were varied using OFAT sweeps to identify the inference subspace boundaries.

Figure 3 shows an OFAT sweep on angle of attack. The vertical lines mark the selected subspace boundaries in angle of attack, which are intended to mark the boundaries of regions where the character of the response surfaces change. There is a trade-off in selecting the subspace boundaries, in that more subspaces mean more individual experimentation regions in procedure four, while fewer subspaces generally require more resources in the data collection and modeling for each subspace. Figures 4 and 5 show OFAT sweeps on sideslip angle and power level, with the selected subspace boundaries marked by vertical lines. All control surface deflections were zero for the sweeps shown in Figures 3-5.

The full independent variable ranges tested are listed in Table 2. Tables 3 and 4, and corresponding Figures 6, 7, and 8, show the definitions of the inference subspaces in terms of boundary values of angle of attack, sideslip angle, and power level. The symmetry of the vehicle was used to justify omitting testing in most of the subspaces with high negative sideslip angles, see Figures 6, 7, and 8. All the subspaces together comprised the full inference space, defined by the full range of the independent variables in Table 2. All control surfaces were tested over their full physical deflection ranges for each subspace.

In the fourth and final procedure, Modern Design Of Experiment (MDOE) techniques[4-6] were applied to each defined subspace in order to obtain the most accurate and complete characterization of the functional dependencies, and also to make sure all interaction effects were adequately modeled. Refs. [2], [4]-[6] describe and demonstrate in detail the advantages of the MDOE approach compared to traditional OFAT for detailed modeling of the functional dependencies, both in terms of the modeling accuracy and in the economy of experimentation resources required to arrive at an acceptable result.

Within each subspace, independent variables were set according to normalized values. Normalized independent variable values are found by mapping the independent variable values in engineering units for each subspace onto the interval [–1,1]. The normalization of each independent variable was implemented by

$$\tilde{x} = -1 + 2\frac{\left(x - x_{min}\right)}{\left(x_{max} - x_{min}\right)} \qquad (1)$$

where $\tilde{x}$ was the normalized value of the independent variable, and the independent variable range in engineering units was $\left[x_{min}, x_{max}\right]$. The inverse transformation was

$$x = x_{min} + \frac{\left(\tilde{x} + 1\right)}{2}\left(x_{max} - x_{min}\right) \qquad (2)$$

All modeling for the inference subspaces was done using normalized values of the independent variables. The final models used for prediction were written in terms of engineering units.

Second-order central composite design[5,6] in four independent variables (for the power-off subspaces) or five independent variables (for the power-on subspaces) was used in each subspace, augmented with a 3rd order D-optimal design[5,6] in the appropriate number of independent variables. A two-dimensional projection of this constellation of data points in normalized independent variable space is shown in Figure 9. The central composite design points occupy the corners, the centers of each face, and the center of the normalized subspace, while the D-optimal points generally fill in between. Although some of the D-optimal points are coincident with the central composite design points, the number of times that this happens is not represented accurately in Figure 9, because of the projection onto two dimensions. This experiment design enabled identification of up to 3rd order functional dependencies and interaction effects. Provisions were made to augment the designed experiment if the data indicated a lack of fit that required modeling functions with higher than 3rd order.

Instrumentation and Data Collection

FASER was used as the wind tunnel model and tested at a nominal flight speed, thus avoiding scaling, Reynolds number, or geometric dissimilarity issues for

comparisons with future flight test data. All control surfaces were instrumented with potentiometers. Air data vanes and airspeed pinwheels were installed on booms attached at each wing tip and extending 1 chord length in front of the wing. The air data sensors, which will be used for flight testing, were calibrated as part of the wind tunnel experiment, since aerodynamic incidence angles and airspeed were carefully controlled and measured in the wind tunnel. The wind tunnel balance was installed near the c.g. of the airplane in the space normally occupied by the accelerometer and rate gyro package during flight test operations.

Control surface deflections and power level were automatically set to the values required by the experiment design via a serial port interface from a laptop computer in the control room to a servomechanism controller onboard on the airplane. The same onboard equipment will be used to command the control surfaces and power level during flight operations. Angle of attack and sideslip angle were set from the control room using servomechanisms driving the movable C-strut in the test section. The angle of attack and sideslip angles were set automatically during OFAT sweeps, but had to be set manually for the MDOE data points, using joystick controllers and a measurement feedback to the control room. Dynamic pressure in the tunnel was regulated to 2 psf by an automatic closed loop control on the wind tunnel fan motor speed.

The experimental set-up was designed to accommodate the MDOE approach, which typically requires changes in more than one independent variable for successive data points. Since the control surface and power level settings were automated using the laptop computer, each data point required only manual setting of angle of attack and sideslip angle using the joysticks in the control room. Each data point was taken as the average of a ten-second dwell using a sampling rate of 100 Hz.

The data for power-on subspaces was collected by interleaving power-on points with power-off points from other subspaces, in order to keep the engine temperature at low levels for extended testing periods. This was necessary to avoid damage to the electric motor. A regulated DC power supply was used to power the electric motor, so that batteries would not have to be swapped in and out. The power-on subspaces were limited to relatively low angle of attack and sideslip angle (see Figure 7), because of excessive vibration of the wind tunnel rig and model for powered runs at high angles of attack and/or high sideslip angles.

The wind tunnel experiment described above was conducted over 4 weeks in May 2002, in the NASA Langley 12-foot Low-Speed Wind Tunnel.

Modeling

Typically, once the experimental data are collected, polynomials in the independent variables are used to model the functional dependence of the output variables on the independent variables, and the model parameters are estimated from the measured data using least squares linear regression[5,6]. The question of which polynomial terms should be included in the model for a given set of data, called model structure determination, gets more difficult with increases in the number of independent variables, increased ranges for the independent variables, or increased complexity of the underlying functional dependency.

Various hypothesis testing techniques[6,7] can be used to identify an adequate model structure, but these methods are iterative and require the involvement of an experienced analyst. Neural networks using radial basis functions with subspace partitioning, or back propagation with layered and interconnected nonlinear activation functions, have also been applied to the response surface modeling problem[8]. For this type of approach, there is a loss of physical insight and a danger of over-fitting the data, because the model structures contain many parameters, typically with no mechanism for limiting the size of the model other than the judgment of the analyst.

In this work, a nonlinear multivariate orthogonal modeling technique[2,3] was used to model response surfaces from wind tunnel data. The technique generates nonlinear orthogonal modeling functions from the independent variable data, and uses those modeling functions with a predicted squared error metric to determine appropriate model structure. The orthogonal functions are generated in a manner that allows them to be decomposed without ambiguity into an expansion of ordinary multivariate polynomials. This allows the identified orthogonal function model to be converted to a multivariate ordinary polynomial expansion in the independent variables, which provides physical insight into the identified functional dependencies.

The next section briefly describes the multivariate orthogonal function modeling approach. In the **Results** section, the multivariate orthogonal function modeling method is applied to identify response surface models for non-dimensional aerodynamic force and moment coefficients for inference subspaces, based on data from the FASER wind tunnel test.

Multivariate Orthogonal Functions

Assume an *N*-dimensional vector of response variable values, $\boldsymbol{y} = \left[y_1, y_2, ..., y_N \right]^T$, modeled in terms of a linear combination of *n* modeling functions $\boldsymbol{p}_j$, $j = 1, 2, ..., n$. Each $\boldsymbol{p}_j$ is an *N*-dimensional vector which in general depends on the independent variables. Then,

$$\boldsymbol{y} = a_1 \boldsymbol{p}_1 + a_2 \boldsymbol{p}_2 + ... + a_n \boldsymbol{p}_n + \boldsymbol{\varepsilon} \tag{3}$$

The a_j, $j = 1, 2, ..., n$ are constant model parameters to be determined, and $\boldsymbol{\varepsilon}$ denotes the modeling error vector. Eq. (3) represents the usual mathematical model used to fit a response surface to measured data from an experiment. We put aside for the moment the important questions of determining how candidate modeling functions $\boldsymbol{p}_j$ should be computed from the independent variables, as well as which candidate modeling functions should be included in Eq. (3), which implicitly determines *n*. Now define an *N*x*n* matrix ***P***,

$$\boldsymbol{P} = \left[\boldsymbol{p}_1, \boldsymbol{p}_2, ..., \boldsymbol{p}_n \right] \tag{4}$$

and let $\boldsymbol{a} = \left[a_1, a_2, ..., a_n \right]^T$. Eq. (3) can be written as a standard least squares regression problem,

$$\boldsymbol{y} = \boldsymbol{P}\,\boldsymbol{a} + \boldsymbol{\varepsilon} \tag{5}$$

The variable $\boldsymbol{\varepsilon}$ represents a vector of errors that are to be minimized in a least squares sense. The goal is to determine $\boldsymbol{a}$ that minimizes the least squares cost function

$$J = \left(\boldsymbol{y} - \boldsymbol{P}\boldsymbol{a} \right)^T \left(\boldsymbol{y} - \boldsymbol{P}\boldsymbol{a} \right) = \boldsymbol{\varepsilon}^T \boldsymbol{\varepsilon} \tag{6}$$

The parameter vector estimate that minimizes this cost function is computed from[3,5-7]

$$\hat{\boldsymbol{a}} = \left[\boldsymbol{P}^T \boldsymbol{P} \right]^{-1} \boldsymbol{P}^T \boldsymbol{y} \tag{7}$$

The estimated parameter covariance matrix is

$$\boldsymbol{Cov}\left(\hat{\boldsymbol{a}} \right) = E\left\{ \left(\hat{\boldsymbol{a}} - \boldsymbol{a} \right) \left(\hat{\boldsymbol{a}} - \boldsymbol{a} \right)^T \right\} = \sigma^2 \left[\boldsymbol{P}^T \boldsymbol{P} \right]^{-1} \tag{8}$$

where E is the expectation operator, and the error variance σ^2 can be estimated from the residuals,

$$\boldsymbol{v} = \boldsymbol{y} - \boldsymbol{P}\hat{\boldsymbol{a}} \tag{9}$$

$$\hat{\sigma}^2 = \frac{1}{\left(N - n \right)} \left[\left(\boldsymbol{y} - \boldsymbol{P}\hat{\boldsymbol{a}} \right)^T \left(\boldsymbol{y} - \boldsymbol{P}\hat{\boldsymbol{a}} \right) \right] = \frac{\boldsymbol{v}^T \boldsymbol{v}}{\left(N - n \right)} \tag{10}$$

and *n* is the number of elements in parameter vector $\boldsymbol{a}$. Parameter standard errors are computed as the square root of the diagonal elements of the $\boldsymbol{Cov}\left(\hat{\boldsymbol{a}} \right)$ matrix from Eq. (8), using $\hat{\sigma}^2$ from Eq. (10).

Estimated model output is

$$\hat{\boldsymbol{y}} = \boldsymbol{P}\,\hat{\boldsymbol{a}} \tag{11}$$

For response surface modeling, the modeling functions (columns of ***P***) are often chosen as polynomials in the measured independent variables. This approach corresponds to using the terms of a Taylor series expansion to approximate the functional dependence of the output response variable on the independent variables.

If the modeling functions are instead multivariate orthogonal functions generated from the measured independent variable data, advantages accrue in the model structure determination for response surface modeling. After the model structure is determined using the multivariate orthogonal modeling functions, each retained modeling function can be decomposed into an expansion of ordinary polynomials in the independent variables. Combining like terms from this final step puts the final model in the form of a Taylor series expansion. It is this latter form of the model that provides the physical insight, particularly in the case of modeling non-dimensional aerodynamic force and moment coefficients. This is the reason that aircraft dynamics and control analyses are nearly always conducted with the assumption of this form for the dependence of the non-dimensional aerodynamic force and moment coefficients on independent variables such as angle of attack and sideslip angle.

Ref. [3] describes a procedure for using the independent variable data to generate multivariate orthogonal modeling functions $\boldsymbol{p}_j$, which have the following important property:

$$\boldsymbol{p}_i^T \boldsymbol{p}_j = 0 \quad , \quad i \neq j \quad , \quad i, j = 1, 2, ..., n \qquad (12)$$

It is also possible to generate multivariate orthogonal functions by first generating ordinary multivariate polynomials in the independent variables, then orthogonalizing these functions using Gram-Schmidt orthogonalization. The process begins by choosing one of the ordinary multivariate polynomial functions as the first orthogonal function:

$$\boldsymbol{p}_1 = \boldsymbol{\xi}_1 \qquad (13)$$

where $\boldsymbol{\xi}_1$ is the ordinary multivariate polynomial function chosen to be the first orthogonal function. Then to make each subsequent ordinary multivariate polynomial function orthogonal to the preceding orthogonal function(s), define the j^{th} orthogonal function $\boldsymbol{p}_j$ as:

$$\boldsymbol{p}_j = \boldsymbol{\xi}_j - \sum_{k=1}^{j-1} \gamma_{kj} \boldsymbol{p}_k \quad j = 2, ..., n \qquad (14)$$

where $\boldsymbol{\xi}_j$ is the j^{th} ordinary multivariate polynomial vector, and the γ_{kj} are scalars determined from

$$\gamma_{kj} = \frac{\boldsymbol{p}_k^T \boldsymbol{\xi}_j}{\boldsymbol{p}_k^T \boldsymbol{p}_k} \qquad \begin{matrix} k = 1, 2, ..., j-1 \\ j = 2, ..., n \end{matrix} \qquad (15)$$

where n is the total number of ordinary multivariate polynomials used as raw material for generating the multivariate orthogonal functions. Eq. (15) results from multiplying both sides of Eq. (13) by $\boldsymbol{p}_k^T$, invoking the mutual orthogonality of $\boldsymbol{p}_k$, $k = 1, ..., j$, and solving for γ_{kj}. It can be seen from Eqs. (13)-(15) that each orthogonal function can be expressed in terms of ordinary polynomial functions. If the $\boldsymbol{p}_j$ vectors and the $\boldsymbol{\xi}_j$ vectors are arranged as columns of matrices $\boldsymbol{P}$ and $\boldsymbol{\Xi}$, respectively, and the γ_{kj} are elements in the k^{th} row and j^{th} column of an upper triangular matrix $\boldsymbol{G}$ with ones on the diagonal, then

$$\boldsymbol{\Xi} = \boldsymbol{P}\boldsymbol{G} \qquad (16)$$

which leads to

$$\boldsymbol{P} = \boldsymbol{\Xi}\boldsymbol{G}^{-1} \qquad (17)$$

The columns of $\boldsymbol{G}^{-1}$ contain the coefficients for expansion of each column of $\boldsymbol{P}$ (i.e., each multivariate orthogonal function) in terms of the ordinary polynomial functions contained in the columns of $\boldsymbol{\Xi}$. Eq. (17) can be used to express each multivariate orthogonal function in terms of ordinary multivariate polynomials.

The orthogonal functions are generated in a manner that allows them to be decomposed without ambiguity into an expansion of ordinary multivariate polynomials. The orthogonalization process can be repeated using arbitrary ordinary multivariate polynomials to generate orthogonal functions of arbitrary order in the independent variables, subject only to limitations related to the information contained in the data. For the FASER wind tunnel data response surface modeling, the orthogonal modeling functions were generated in the manner described above.

If an additional independent variable is introduced to represent blocking in the experiment, the orthogonal function modeling can be used to orthogonalize the block effects with respect to the other independent variable effects. A blocking variable is typically used to indicate some change in the experimental conditions that cannot be controlled by the experimenter. The blocking variable to the first power can simply be made one of the ordinary polynomial vectors $\boldsymbol{\xi}_j$. The orthogonalization procedure in Eqs. (13)-(15) makes the blocking variable orthogonal to the other orthogonal modeling functions, which are generated from ordinary multivariate polynomial functions. This approach allows arbitrary blocking of the data points in the experiment using analytical means alone. Normally, experiment designers try to arrange the normalized settings of the independent variables so that the blocking variable is orthogonal to the other independent variables and their polynomial combinations. This separates the block effect from the other model terms and allows identification of a block effect independent of the other terms in the model. However, with the analytical orthogonal blocking described above, the blocking variable is made orthogonal to the other modeling functions analytically, so that arranging the experiment so that independent variable settings and their polynomial combinations are orthogonal to the blocking variable is not necessary. All the models identified in this work included an analytic blocking variable that accounted for drift in experimental conditions between the time when the central composite design points were collected and the time when the D-optimal design points were collected.

With the modeling functions orthogonal, using Eqs. (4) and (12) in Eq. (7), the j^{th} element of the estimated parameter vector $\hat{\boldsymbol{a}}$ is given by

$$\hat{a}_j = \left(\boldsymbol{p}_j^T\ \boldsymbol{y}\right) \Big/ \left(\boldsymbol{p}_j^T\ \boldsymbol{p}_j\right) \tag{18}$$

Combining Eqs. (4), (6), and (11)-(12),

$$\hat{J} = \boldsymbol{y}^T \boldsymbol{y} - \sum_{j=1}^{n} \hat{a}_j^2 \left(\boldsymbol{p}_j^T\ \boldsymbol{p}_j\right) \tag{19}$$

or, using Eq. (18),

$$\hat{J} = \boldsymbol{y}^T \boldsymbol{y} - \sum_{j=1}^{n} \left(\boldsymbol{p}_j^T\ \boldsymbol{y}\right)^2 \Big/ \left(\boldsymbol{p}_j^T\ \boldsymbol{p}_j\right) \tag{20}$$

Eq. (20) shows that when the modeling functions are orthogonal, the reduction in the estimated cost resulting from including the term $a_j\ \boldsymbol{p}_j$ in the model depends only the dependent variable data $\boldsymbol{y}$ and the added orthogonal modeling function $\boldsymbol{p}_j$. This decouples the least squares modeling problem, and makes it possible to evaluate each orthogonal modeling function in terms of its ability to reduce the least squares model fit to the data, regardless of which other orthogonal modeling functions are present in the model. When the modeling functions $\boldsymbol{p}_j$ are instead polynomials in the independent variables (or any other non-orthogonal function set), the least squares problem is not decoupled, and iterative analysis is required to find the subset of modeling functions for an adequate model structure.

The orthogonal modeling functions to be included in the model are chosen to minimize predicted squared error *PSE*, defined by[9]

$$PSE = \frac{\left(\boldsymbol{y} - \boldsymbol{P}\hat{\boldsymbol{a}}\right)^T \left(\boldsymbol{y} - \boldsymbol{P}\hat{\boldsymbol{a}}\right)}{N} + 2\,\sigma_{max}^2 \frac{n}{N} \tag{21}$$

or

$$PSE = \frac{\hat{J}}{N} + 2\,\sigma_{max}^2 \frac{n}{N} \tag{22}$$

where σ_{max}^2 is the maximum variance of elements in the error vector $\boldsymbol{\varepsilon}$, assuming the correct model structure, and n is the number of model terms. The *PSE* in Eq. (22) depends on the mean squared fit error $\hat{J}/N$, and a term proportional to the number of terms in the model, n. The latter term prevents over-fitting the data with too many model terms, which is detrimental to model prediction accuracy[9]. The factor of 2 in the model over-fit penalty term accounts for the fact that the *PSE* is being used when the model structure is not correct, i.e., during the model structure determination stage. Ref. [9] contains further justifying statistical arguments and analysis for the form of *PSE* in Eqs. (21)-(22). Note that while the mean squared fit error $\hat{J}/N$ must decrease with the addition of each orthogonal modeling function to the model (by Eq. (19) or (20)), the over-fit penalty term $\sigma_{max}^2\, n/N$ increases with each added model term (n increases). Introducing the orthogonal modeling functions into the model in order of most effective to least effective in reducing the mean squared fit error (quantified by $\hat{a}_j^2 \left(\boldsymbol{p}_j^T\ \boldsymbol{p}_j\right)$ for the j^{th} orthogonal modeling function) means that the *PSE* metric will always have a single global minimum value. Figure 10 depicts this graphically, using actual modeling results from Ref. [2]. Ref. [9] contains details on the statistical properties of the *PSE* metric, including justification for its use in modeling problems.

For wind tunnel testing, repeated runs at the same test conditions are often available. If σ_o^2 is the output variance estimated from measurements of the output for repeated runs at the same test conditions, then σ_{max}^2 can be estimated as

$$\sigma_{max}^2 \doteq 25\ \sigma_o^2 \tag{23}$$

If the output errors were Gaussian, Eq. (23) would correspond to conservatively placing the maximum output variance at 25 times the estimated value (corresponding to a $5\sigma_o$ maximum deviation). However, the estimate of σ_o^2 may not be very good, because of relatively few repeated runs available or errors in the independent variable settings or drift errors when duplicating test conditions for the repeat runs. The $5\sigma_o$ value was found to give the most accurate models in model identification algorithm testing done using simulated data. In Ref. [2], the model structure determined using *PSE* was found to be virtually the same for σ_{max}^2 in the range:

$$9\ \sigma_o^2 \le \sigma_{max}^2 \le 100\ \sigma_o^2 \tag{24}$$

This happens because the plot of mean square fit error versus added orthogonal modeling functions is typically very flat in the region of minimum *PSE*, see Figure 10.

Using orthogonal functions to model the response variable made it possible to evaluate the merit of including each modeling function *individually* as part of the model, using the predicted squared error *PSE*. Since the goal is to select a model structure with minimum *PSE*, and the *PSE* always has a single global minimum for orthogonal modeling functions, the model structure determination was a well-defined and straightforward process that could be (and was) automated.

After the orthogonal modeling functions that minimized *PSE* were selected, each retained orthogonal function was expanded into an ordinary polynomial expression, and common terms in the ordinary polynomials were combined using double precision arithmetic to arrive finally at a multivariate model using only ordinary polynomials in the independent variables. Ordinary polynomial terms that contributed less than 0.1 percent of the final model root-mean-square magnitude were dropped.

Orthogonal modeling functions are useful in determining the model structures for the response variables using the *PSE* metric, by virtue of the properties of orthogonal modeling functions and the resultant decoupling of the associated least squares problem. The subsequent decomposition of the retained orthogonal functions is done to express the results in physically meaningful terms and to allow analytic differentiation for partial derivatives of the response variable with respect to the independent variables.

Results

Figures 11, 12, and 13 show results for the response surface model fits to measured lift, drag, and pitching moment coefficient data obtained by applying the multivariate orthogonal function nonlinear modeling technique to experimental data from longitudinal subspace 16 for the FASER wind tunnel test. The crosses shown in the top plot of the figures are measured data, and the circles are values computed from the identified response surface models. Values for σ_o^2 were found from twelve repeated runs at the normalized center point of the independent variable ranges, using the method described above. Model structure determination and parameter estimation were done automatically using the orthogonal function modeling technique. The orthogonal function modeling software allows manual override by the analyst in the model structure determination stage, but this option was not used for the results presented here. All data analysis and modeling was done on a 1.2 GHz personal computer running MATLAB® 6.5. The orthogonal modeling technique described above was implemented as an m-file function.

The model residuals shown in the middle plot of Figures 11, 12, and 13 show a random character with magnitudes on the order of the noise level estimated from repeated runs. The dashed lines in the middle and lower plots in the figures represent $\pm 2\sigma_0$, computed from repeated runs at the subspace center point. The lower plots in the figures show that the prediction residual magnitudes are also within the estimated noise levels for the output responses. Results shown for this subspace were typical.

Table 5 contains the identified model structures for C_D, C_L, and C_m for this inference subspace. Based on the data, the identification algorithm determined that no sideslip angle dependence was needed for the longitudinal coefficients models in subspace 16, so the final models did not include sideslip angle.

The results shown in Figures 11, 12, and 13 and the associated analysis of residuals indicated that the functional dependencies were accurately captured by the response surface models identified using the experiment design and modeling techniques described. Similar results were generated for the other longitudinal and lateral/directional subspaces listed in Tables 3 and 4, and depicted in Figures 6, 7, and 8.

Figure 14 shows a screen capture of a 3D plotting tool developed to inspect the response surface fits to

measured data. The symbols represent the measured data points, and the smooth surface is the identified response surface. The viewpoint for the 3D plot can be rotated and zoomed in or out, under the control of the analyst, and the two independent variables for the 3D plotting can be selected from the complete set of independent variables. This tool gives a good overview of the response surface topology, using 3D slices through the inference space.

Concluding Remarks

This paper describes and demonstrates an efficient and effective approach to developing a wind tunnel database for a research model airplane. The use of OFAT sweeps for subspace definition proved useful in defining subspace boundaries and as trial runs to identify and resolve problems related to experimental procedure, data collection, and instrumentation. The use of multivariate orthogonal modeling functions simplified the model structure determination problem and allowed arbitrary orthogonal blocking. The quality of the modeling and prediction results from the experiment design and modeling approach described and used were excellent. However, because the wind tunnel was not set up for MDOE experimentation, the overall efficiency of the testing was not what it could have been.

Significant efficiency improvement would accrue if the data could be transferred to a computer for analysis in real time, and if the wind tunnel rig could be set automatically to arbitrary angles of attack and sideslip angles. In this case, the modeling software could automatically determine the model structure and parameter values in real time as each data point is taken, then compute model fit metrics and make 3D plots. The augmentation of the MDOE experiment designs for higher order model fits, or the re-definition of subspace boundaries could be automated as well, resulting in a testing operation where the human analyst would be needed only to provide high-level oversight of the entire operation.

References

1. Monzon, B.R. "Development of a Nonlinear Simulation for a Research Model Airplane," MSE Thesis, George Washington University JIAFS, NASA Langley Research Center, September 2001.

2. Morelli, E.A. and DeLoach, R. "Response Surface Modeling using Multivariate Orthogonal Functions," AIAA paper 2001-0168, 39th AIAA Aerospace Sciences Meeting and Exhibit, Reno, Nevada, January 2001.

3. Morelli, E.A., "Global Nonlinear Aerodynamic Modeling using Multivariate Orthogonal Functions," *Journal of Aircraft*, Vol. 32, No. 2, March-April 1995, pp. 270-77.

4. DeLoach, R. "Applications of Modern Experiment Design to Wind Tunnel Testing at NASA Langley Research Center," AIAA 2000-2639, *36th AIAA Aerospace Sciences Meeting and Exhibit*, Reno, NV, January 1998.

5. Box, G.E.P., Hunter, W.G., and Hunter, J.S., *Statistics for Experimenters – An Introduction to Design, Data Analysis, and Model Building*, John Wiley & Sons, Inc., New York, NY, 1978, Chapter 14.

6. Montgomery, D.C., *Design and Analysis of Experiments*, 5th Ed., John Wiley & Sons, New York, NY, 2001.

7. Klein, V., Batterson, J.G., and Murphy, P.C., "Determination of Airplane Model Structure from Flight Data by Using Modified Stepwise Regression," NASA TP-1916, 1981.

8. Lo, C.F., Zhao, J.L., and DeLoach, R., "Application of Neural Networks to Wind Tunnel Data Response Surface Methods," AIAA 2000-2639, *21st AIAA Aerodynamic Measurement Technology and Ground Testing Conference*, Denver, CO, June 2000.

9. Barron, A.R., "Predicted Squared Error : A Criterion for Automatic Model Selection," *Self-Organizing Methods in Modeling*, Farlow, S.J., Ed., Marcel Dekker, Inc., New York, NY, 1984, pp. 87-104.

10. *Using MATLAB*, Version 6.1, The MathWorks, Inc., Natick, MA, 2001.

Table 1 FASER Wind Tunnel Experiment Procedures

Procedure	Description
1	Power sweep with wind off for static thrust modeling
2	Angle of attack sweeps at min, max, and zero elevator, for static stability and trim
3	Angle of attack, sideslip angle, and power sweeps for inference subspace identification
4	2nd order central composite design and 3rd order D-optimal design for inference subspace modeling

Table 2 Independent Variable Ranges

Variable	α	β	pwr	δ_e	δ_a	δ_r	δ_f
Min	–7.5	–30	0	–25	–25	–30	0
Max	80	30	100	25	25	30	30
Units	deg	deg	%	deg	deg	deg	deg

Table 3 Longitudinal Inference Subspaces

Inference Subspace	Angle of Attack (deg)		Power Level (percent)		Sideslip Angle (deg)	
	min	max	min	max	min	max
13	–7.5	10	0	0	–10	10
23	–7.5	10	0	100	–10	10
6	–7.5	10	0	0	10	30
15	10	20	0	0	–10	10
17	10	20	0	0	10	30
24	10	20	0	100	–10	10
16	20	40	0	0	–10	10
18	20	40	0	0	10	30
5	40	80	0	0	–10	10
4	40	80	0	0	10	30

Table 4 Lateral/Directional Inference Subspaces

Inference Subspace	Angle of Attack (deg)		Power Level (percent)		Sideslip Angle (deg)	
	min	max	min	max	min	max
7	–7.5	10	0	0	–10	10
8	–7.5	10	0	0	10	30
26	–7.5	10	0	0	–30	–10
19	10	20	0	0	–10	10
20	20	40	0	0	–10	10
21	10	20	0	0	10	30
22	20	40	0	0	10	30
11	40	80	0	0	–10	10
10	40	80	0	0	10	30

Table 5 Longitudinal Subspace Identified Model

Inference Subspace	Model Structure
16	$C_D = a_0 + a_1\alpha^2 + a_2\alpha\delta_e + a_3\delta_f$
	$C_L = b_0 + b_1\delta_e + b_2\delta_f + b_3\alpha\delta_e + b_4\alpha^2 + b_5\alpha\delta_f^2$
	$C_m = c_0 + c_1\delta_e + c_2\alpha^2 + c_3\delta_f + c_4\alpha\delta_e + c_5\alpha\delta_e^2 + c_6\alpha$

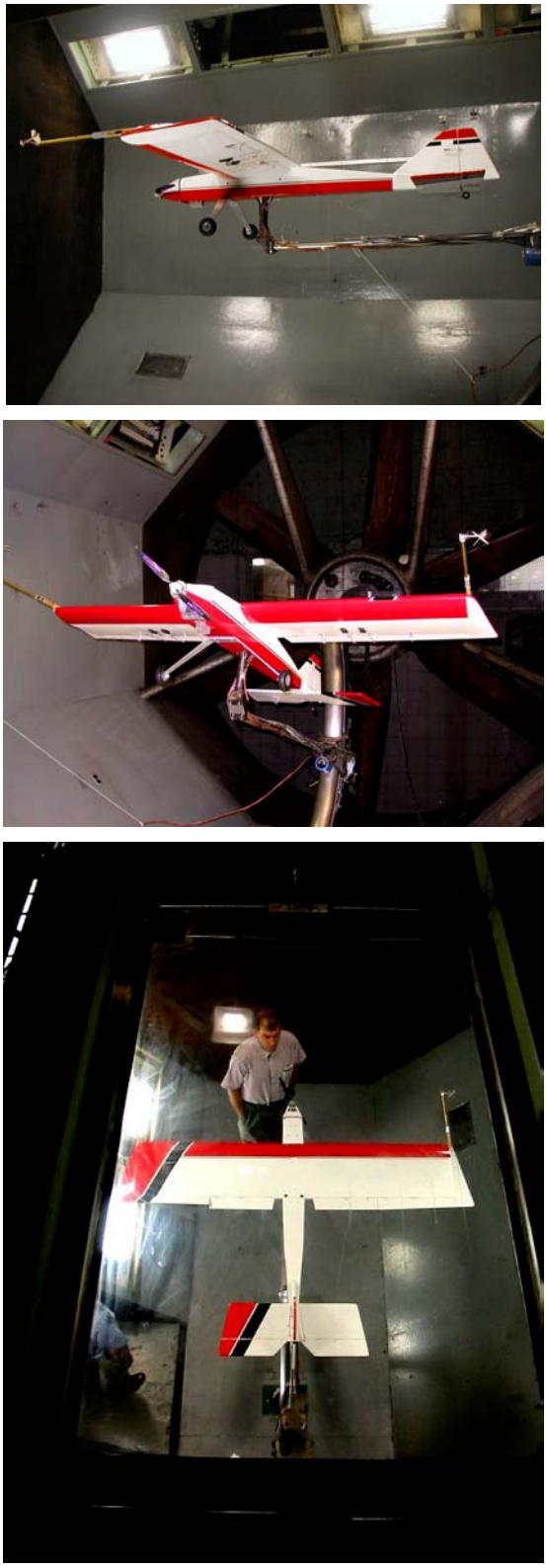

Figure 1 Free-flying Airplane for Sub-scale Experimental Research (FASER) in the NASA Langley 12 ft Low-Speed Wind Tunnel

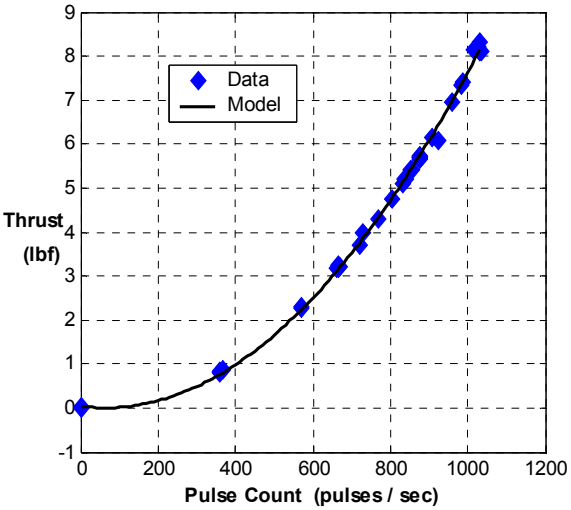

Figure 2 Static Engine Thrust, Wind Tunnel Air Off

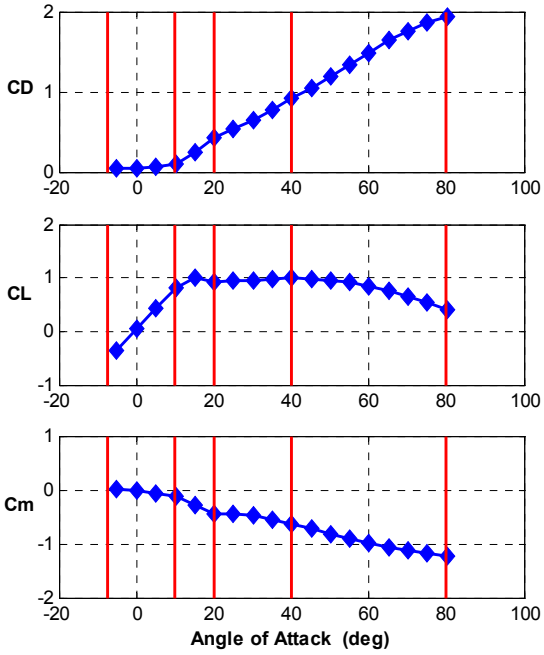

Figure 3 Angle of Attack Sweep for Subspace Boundary Definition, β=0, *pwr*=0

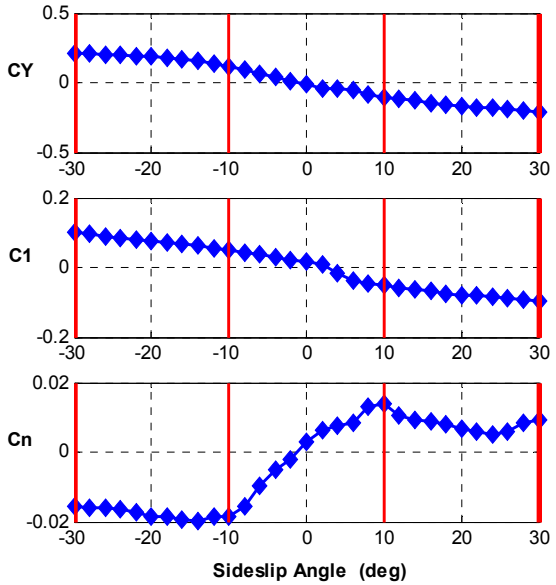

Figure 4 Sideslip Angle Sweep for Subspace Boundary Definition, α=80, *pwr*=0

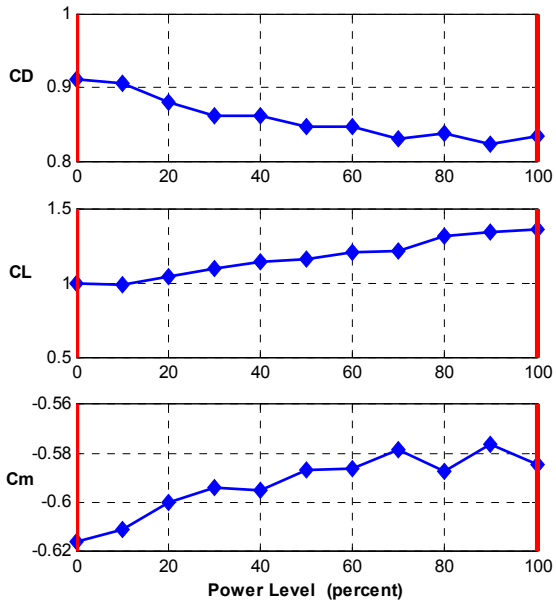

Figure 5 Power Sweep for Subspace Boundary Definition, α=40, β=0

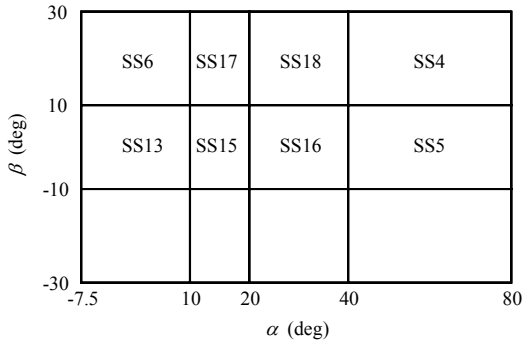

Figure 6 Longitudinal Subspaces, Power Off

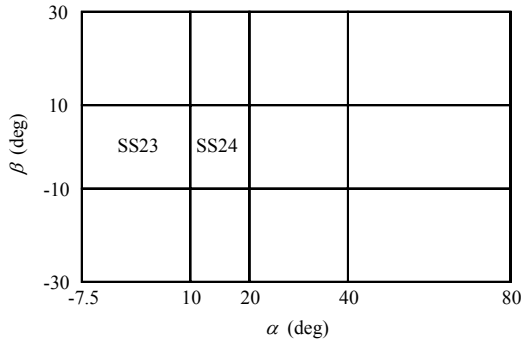

Figure 7 Longitudinal Subspaces, Power On

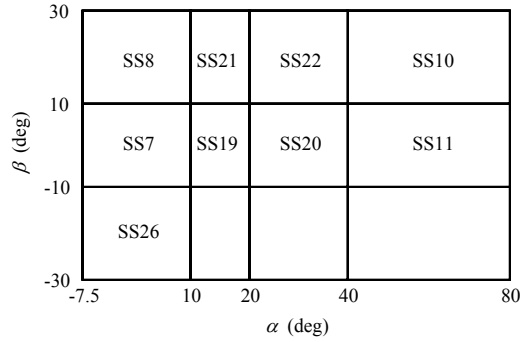

Figure 8 Lateral/Directional Subspaces, Power Off

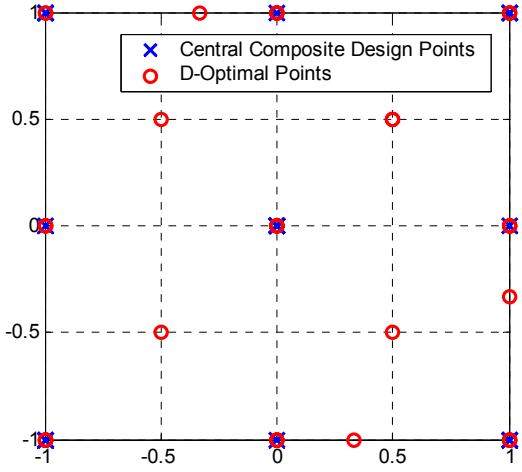

Figure 9 Experiment Design Projection onto Two Dimensions

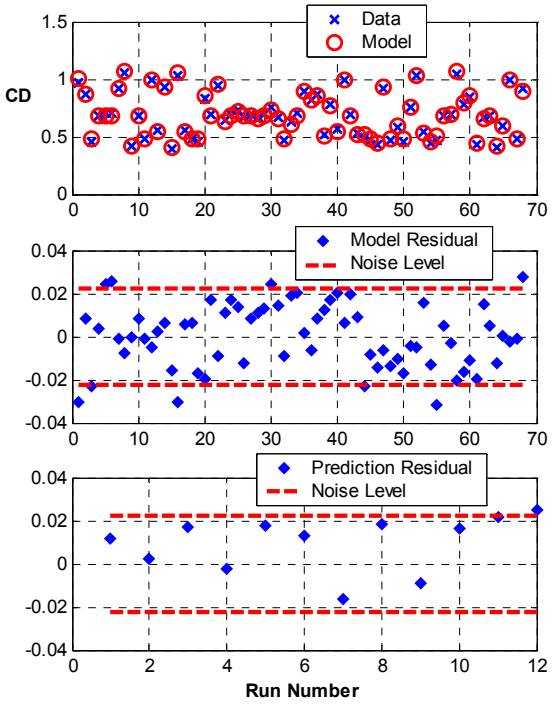

Figure 11 Modeling and Prediction Results for Drag Coefficient, Longitudinal Subspace 16

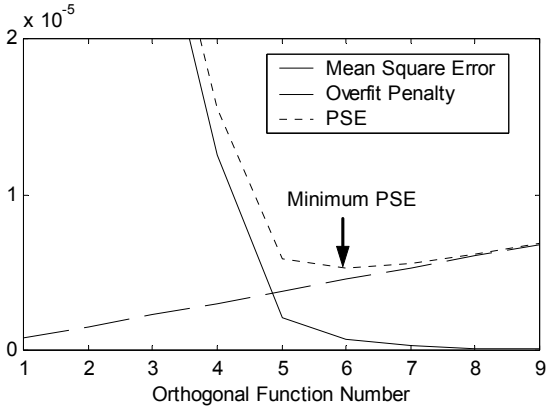

Figure 10 Predicted Squared Error (*PSE*) Components

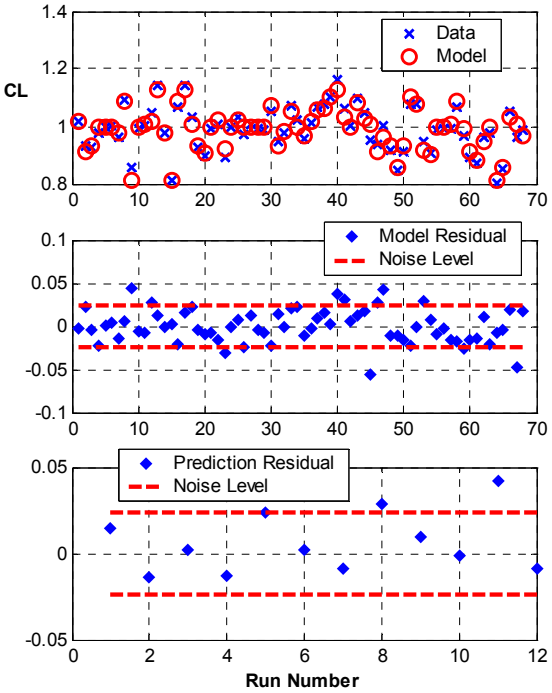

Figure 12 Modeling and Prediction Results for Lift Coefficient, Longitudinal Subspace 16

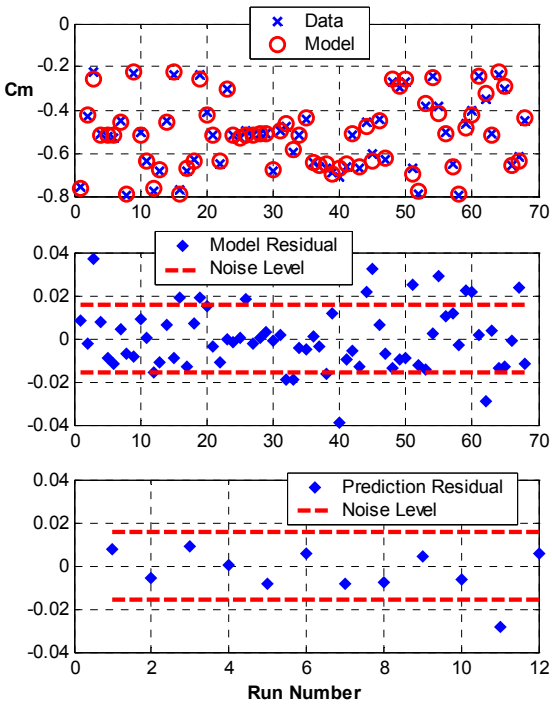

Figure 13 Modeling and Prediction Results for Pitching Moment Coefficient, Longitudinal Subspace 16

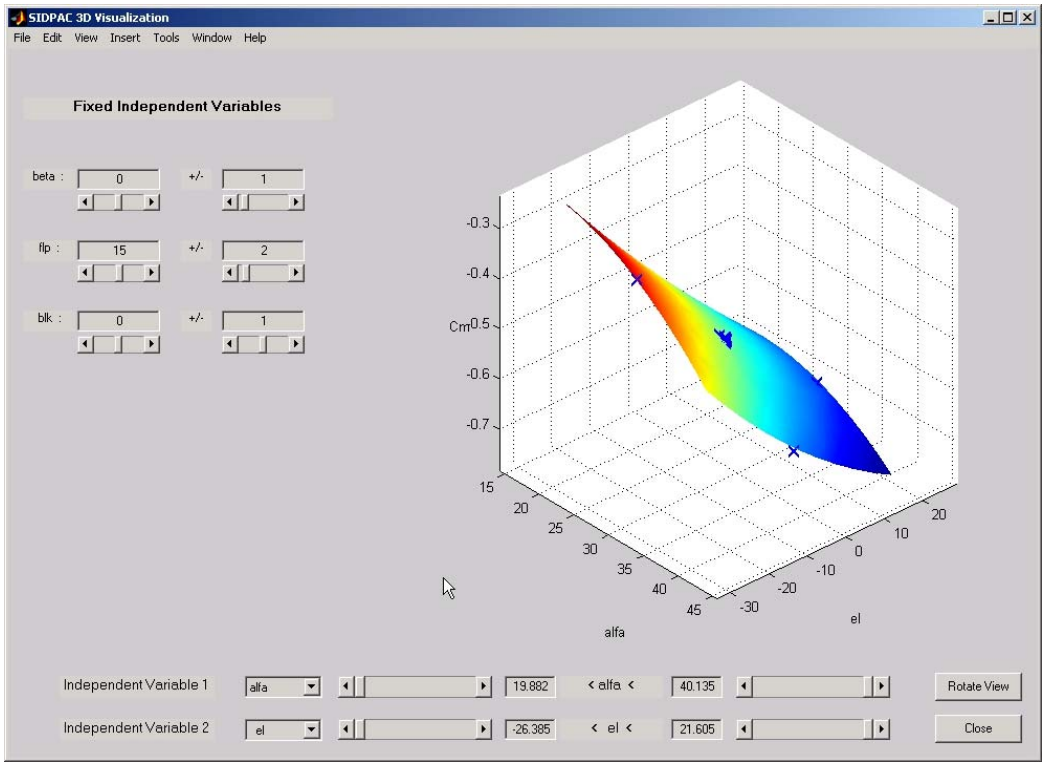

Figure 14 3D Plotting Tool using Pitching Moment Cofficient for Longitudinal Subspace 16